ACS OMEGA

http://pubs.acs.org/journal/acsodf

Article

Investigation of the Three-Dimensional Hybrid Casson Nanofluid Flow: A Cattaneo−Christov Theory

Asad Ullah,* Ramadan A. ZeinEldin, and Hamiden Abd El-Wahed Khalifa

Cite This: *ACS Omega* 2023, 8, 10991−11002

Read Online

ABSTRACT: We consider the Casson hybrid nanofluid (HN) (ZnO + Ag/Casson fluid) that flows steadily along a two-directional stretchable sheet under the influence of an applied changing magnetic flux and is electrically conducting. The basic Casson and Cattaneo−Christov double diffusion (CCDD) formulations are used for the simulation of the problem. This is the first study on the analysis of the Casson hybrid nanofluid by using the CCDD model. The use of these models generalize basic Fick's and Fourier's laws. The current produced due to the magnetic parameter is taken into consideration by using the generalized Oham law. The problem is formulated and then transformed to a coupled set of ordinary differential equations. The simplified set of equations is solved using the homotopy analysis method. The obtained results are presented through tables and graphs for various state variables. A comparative survey in all the graphs is presented for the nanofluid (ZnO/Casson fluid) with the HN (ZnO + Ag/Casson fluid). These graphs depict the effect of various pertinent parameters, like Pr, M, Sc, γ, Nt, m, Nb, δ_1, and δ_2, varying values over the flow. The Hall current parameter m and stretching ratio parameter γ show increasing trends for the velocity gradient, while the magnetic parameter and the flux of mass depict opposite trends for the same profile. The increasing values of the relaxation coefficients show an opposite trend. Furthermore, the ZnO + Ag/Casson fluid shows a good performance in the transfer of heat and thus can be used for cooling purposes to increase the efficiency of the system.

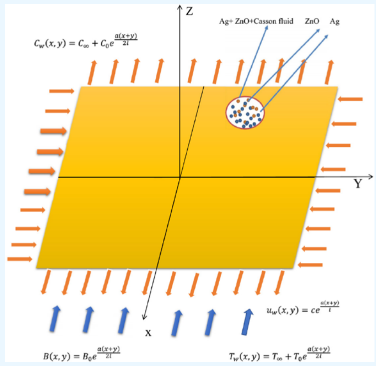

1. INTRODUCTION

The study of the phenomena of heat energy and mass transport has attracted researchers for the last few decades. The main idea behind this trend is their applications in various fields of technology. With the passage of time, new ideas were introduced and the effectiveness of tools is strengthened day by day. One such tool is the suspension of nanomaterial(s) in host fluid. This idea is given by Choi.[1] The size of these nanoparticles varies from 1 to 100 nm. Results in the literature have proved that the smaller the size of the nanoparticles, more effective are its results.[2] The idea of nanofluids opened a new door, where investigations have been started to prepare these nanofluids both at industry and laboratory levels. Rashidi et al.[3] studied the roughness of the surface for condensation flow inside microchannels. In that work, they established a relation between surface roughness and condensation and reported that condensation varies only with the height and roughness of the surface. Mansoury et al.[4] analyzed Al_2O_3 + H_2O nanofluid flow inside the parallel heat exchangers. In this analysis, they reported a 26% increase in the transfer rate of heat energy for 1% addition of the nanoparticles. A T-shape square cavity having pores was examined by Hatami et al.[5] for the optimal heat transfer rate by using the finite element method (FEM). The impact of various nanoparticles on the Nusselt number is discussed with contour plots by implementing response surface methodology. A more recent survey can be found in refs 6−8.

The results discussed above form the aim in the literature to elaborate a single type of nanoparticle mixed with a conventional fluid. Recently, the thermal conduction capability of a hybrid type fluid was studied by Jin et al.[9] This work plays a key role in providing a base for the use of the hybrid nanofluid (HN; fluid that contains nanoparticles of different kinds) in academia. A comparative analysis of hybrid and common nanofluids is presented in this study. Furthermore, they recommended a massive enhancement in the transfer of heat analysis for the HN. Hybrid nanofluids are less expensive, are easily available, and have many applications in industry as well as in engineering and technology.[10] The aluminum and SiO_2 composition of H_2O based HNs for the impact of the nanoparticle concentration on the transfer of heat is examined by Yıldız et al.[11] This study recommends a higher thermal energy transfer subject to improved nanoparticle concentration. Also, the nanoparticle volume fraction augments the transfer of heat with its minimal size. An experimental analysis

Received: December 5, 2022
Accepted: February 28, 2023
Published: March 14, 2023

https://doi.org/10.1021/acsomega.2c07750
ACS Omega 2023, 8, 10991−11002

of a hybrid nanofluid ($Cu-Al_2O_3$/water) for studying the rheological properties and the transfer of heat is performed by Asokan et al.,[12] followed by Ho et al.,[13] who performed a comparative analysis of microencapsulated phase change material (MEPCM) and phase change material (PCM) nanoparticles for the transfer of heat and concentration. Their study shows a better performance of MEPCM nanoparticles in both analyses. A more brief survey on HNs including experimental analysis can be found in refs 14−19.

In the last few decades various approaches, geometries, and assumptions have been made for the analysis of fluid flow problems. Among them, one inclusion is boundary layer conducting magnetohydrodynamic (MHD) fluid flow. Khan[20] analyzed molybdenum disulfide nanofluid flow impacted by the presence of a magnetic field for heat transfer enhancement treatment. Similarly, Chamkha et al.[21] undertook the mixed convection motion through a square enclosure by employing a magnetic field. The non-Newtonian Buongiorno model for two-phase flow inside a pipe is reported by Alsabery et al.[22] They considered aluminum nanoparticles inside water and analyzed the impact of a magnetic field on various state variables. The enhancing trend due to the impact of a magnetic field in the analysis of the non-Newtonian fluid flow past a wedge is reported by Muhammad et al.[23] This study recommends an increasing velocity profile with higher microorganisms. The MHD flow through a perforated medium was studied by Siddiqui and Sheikholeslami.[24] The results are displayed through contour plots for parameters, like Hartmann and Reynolds numbers. The study recommends a decreasing pattern in the boundary layer thickness for larger values of the volume fraction and the Reynolds number. Sheikholeslami[25] used the lattice Boltzmann method (LBM) for the three-dimensional flow in the existence of a magnetic field. In this study, he analyzed the impact of Lorentz forces on the temperature profile. The generation of entropy inside an enclosure during three-dimensional natural convective flow was studied by Seyyedi et al.[26] by using control volume FEM (CVFEM). Also, a briefer survey of nanofluid flow and entropy generation during the rotating frame is presented by Khan et al.[27]

In the past few years boundary layer flow past a stretchable surface has been examined by different researchers. The aim behind this analysis is the applications of the boundary layer flow that varies from metallurgy, to coatings of various sheets, to drawing and tinning of wires. This idea was first given by Sakiadis,[28] which was further undertaken by Crane[29] in the case of stretching sheet. A more physical description with inclusion of the boundary restriction is given in refs 30 and 31. The cases of suction/injection and the to-and-fro motion of the sheet are analyzed by Magyari et al.[32] and Wang[33] for the liquid film. A few years later Miklavčič and Wang[34] explained the exact solution of the unstable sheet. In their reports they found that the surface stability is directly linked with the mass suction. Similar reports were presented by Bhattacharyya[35] for the exponential expanding surface. The case of stagnation point motion of a nanofluid along an extendable sheet is presented by Bachok et al.[36] A more recent survey by considering the same geometry is presented in refs 37−40.

Models used to study fluid flow are constituted to explain the flow of a certain fluid in a more accurate way. These models are classified as Newtonian and non-Newtonian fluids in the literature.[41] Some basic laws, like Fourier's and Fick's, play a vital role in fluid flow problems.[42] These laws are modified for the convection derivative of time to obtain the Cattaneo−Christov model.[43] Irfan et al.[44] examined Carreau fluid migration by considering the Cattaneo−Christov double diffusion (CCDD) model for varying thermal conduction. The thermal transport of Burgers nanofluid is examined by Iqbal et al.[45] using the CCDD model. The applications of non-Newtonian fluids are in abundance in the literature as compared to the common Newtonian fluids. In this class one such an important fluid is the Casson fluid, which has a mathematical relation for the shear stress. The relation was introduced by Casson[46] for the analysis of a printing ink−oil suspension. High shear viscosity, thinning, and yield stress are the most important properties of this fluid.[47] This model behaves like a Newtonian fluid at higher wall stress as compared to the yield stress. In 2007, Mitsoulis[48] presented details of the behavior of the deformation rate of the Casson stress tensor. Some of the benchmark problems are reviewed and the flow over different surfaces are analyzed in this work. This work plays a key role in the area of fluid mechanics. Non-Newtonian fluid flow past a stretching sheet has many applications in the area of heat and mass transfer analysis.[49] The Soret and Dufour effects for a magnetohydrodynamic fluid flow past an expanding surface were investigated by Reddy et al.[50] Goud Bejawada et al.[51] studied the heat and mass transfer for the Casson fluid flow past an inclined Forchheimer porous moving plate. The thermophysical properties of the Casson fluid flow past an inclined surface are reported by Ramzan et al.[52] In this work they studied various effects, like Dufour, Soret, and chemical reaction. More relevant work on this fluid can found in refs 53 and 54. The CCDD model for the to-and-fro and oscillatory motion of the sheet by considering the stretched and micropolar fluid migration was studied by Ahmad et al.[55] and Rauf et al.,[56] respectively. For the analysis of the expanding surface by taking the Walters-B and Prandtl fluid flow, Hayat et al.[57,58] used the CCDD model. In these reports the source and sink of heat are explained. A more detailed survey on the CCDD model can be found in refs 59−62.

The behavior of the Casson fluid flow and its applications at higher and lower shear rates attract researchers. These applications vary from drilling processes to bioengineering and food processing. Mabood et al.[63] studied the magnetic field impact of the Casson fluid flow past a stretching surface. They examined the thermal radiation impact by considering the surface as porous. Anwar et al.[64] analyzed the variable wall temperature for the natural convective unsteady MHD Casson fluid flow. The impact of radiation and suction/injection are described in this study. Sandeep et al.[65] presented a detailed survey by analyzing the chemically reactive Casson fluid flow past a curved heated surface. Saleem et al.[66] studied the Casson fluid flow inside a tube. The tube wall was considered wavy and stretchable. Hafeez et al.[67] presented the impact of rotation during the MHD Casson fluid flow though a surface having an inclination. In this work, the peristaltic transport is also considered for fluid flow. Alzahrani et al.[68] studied the viscous impact of the Casson fluid flow past a rotating channel. The variable thermal conductivity and thermal radiation impact are briefly explained by Rehman et al.[69] In this work they examined non-Newtonian behavior in various flow regimes.

In view of the literature presented above, the goal of this work is to elaborate the conducting 3D Casson fluid flow past a bistretching sheet by considering the CCDD model in a

https://doi.org/10.1021/acsomega.2c07750
ACS Omega 2023, 8, 10991−11002

variable magnetic field. The thermal energy and mass transfer analysis with the impact of the current produced during the HN migration are taken into account. The work aims to generalize the Fourier and Fick laws. This is the first attempt to analytically study the 3D Casson fluid flow for the two-way-stretching surface in a variable magnetic field by considering the CCDD model. The article is divided into five main sections, where sections 2 and 3 explain the formulation of the problem and solution strategy. The obtained results are discussed in section 4, whereas discussion of the tables and conclusions are presented in sections 5 and 6, respectively.

2. PROBLEM FORMULATION

Assume the non-Newtonian Casson HN (Ag + ZnO + Casson fluid) motion past an expanding surface in the x- and y-directions with $u_w = ce^{(x+y/l)}$ and $v_w = de^{(x+y/l)}$, respectively. In u_w and v_w, l is the sheet length and c and d are the velocity references. The flow is incompressible and steady. The schematic diagram is assumed in such a way in the Cartesian system of coordinates that its midpoint originates at the origin as presented in Figure 1. A time dependent magnetic field is

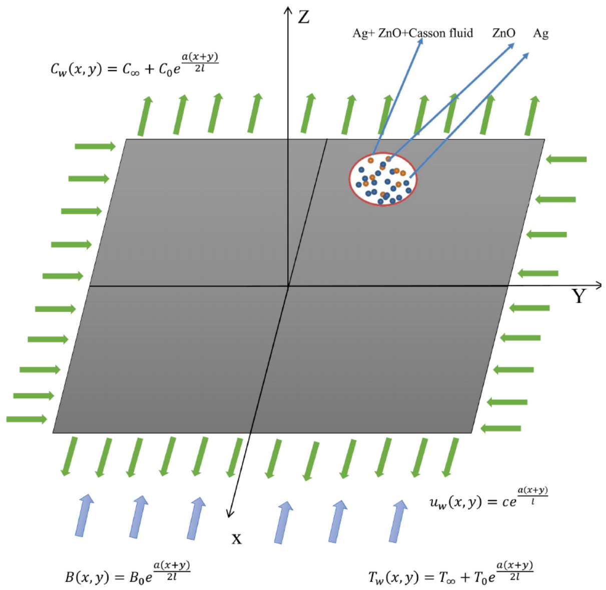

Figure 1. Problem geometry.

applied at an angle of 90° to the surface of the geometry chosen. The concentration and wall temperature are given by the relations

$$C_w - C_\infty = C_0 \exp\left(\frac{a(x+y)}{2l}\right)$$

and

$$T_w - T_\infty = T_0 \exp\left(\frac{a(x+y)}{2l}\right)$$

respectively. The current produced due to the applied magnetic field is taken into account. This current is mathematically given by the following relations.[70]

$$\tilde{j} + \frac{\omega_e}{B_0 t_e} \times (\tilde{j} \times \tilde{B}) = \sigma_{hnf}(\tilde{E} + \tilde{V} \times \tilde{B}) - \frac{\sigma_{nf} P_e}{e n_e} \quad (1)$$

where $\tilde{B}$ is the magnetic field having strength B_0, $\tilde{V}$ is the velocity, $\tilde{E}$ is the electric field strength, $\tilde{j}$ is the current density, n_e and e are the electron number density and charge, P_e is the pressure of electrons, σ_{hnf} is the HN electrical conductivity, t_e is the electron collision time, and ω_e is the electron frequency, respectively. There is no external voltage applied to the fluid flow, so as a result we take $\tilde{E} = 0$. Also, $\tilde{j}$ is constant; therefore, $\nabla \cdot \tilde{j} = 0$. Furthermore, the current density is constant during the flow region and is zero along the z-axis.

Furthermore, we assume the rheological relation for the incompressible Casson fluid as follows:[71]

$$\tau_{ij} = \begin{cases} 2e_{ij}\left(\mu_b + \dfrac{p_y}{\sqrt{2\varpi}}\right) & \text{for } \varpi > \varpi_c \\ 2e_{ij}\left(\mu_b + \dfrac{p_y}{\sqrt{2\varpi_c}}\right) & \text{for } \varpi < \varpi_c \end{cases}$$

Here, ϖ_c is the non-Newtonian model critical value, e_{ij} is the rate of deformation, p_y is the stress yield, and $\varpi = e_{ij}e_{ij}$.

The heat transfer and mass transfer are formulated with the CCDD model for the generalization of the Fick and Fourier laws:[43,72]

$$\tilde{q} + k\nabla T = -\lambda_e(\tilde{q}_t + \tilde{V}\cdot\nabla\tilde{q} - \tilde{q}\cdot\nabla\tilde{V} + (\nabla\cdot\tilde{V})\tilde{q}) \quad (2)$$

$$\tilde{J} + D_B\nabla C = -\lambda_c(\tilde{J}_t + \tilde{V}\cdot\nabla\tilde{J} - \tilde{J}\cdot\nabla\tilde{V} + (\nabla\cdot\tilde{V})\tilde{J}) \quad (3)$$

Here, $\tilde{J}$ and $\tilde{q}$ represent the mass and heat fluxes, D_B represents the Brownian motion, T (C) denotes the temperature (concentration), k is the thermal conductivity, and λ_c (λ_e) represents the concentration (energy relaxation) parameter, respectively.

In view of the above assumptions, the steady Casson hybrid nanofluid flow with the CCDD model takes the following forms:[57,73]

$$\frac{\partial u}{\partial x} + \frac{\partial v}{\partial y} + \frac{\partial w}{\partial z} \quad (4)$$

$$u\frac{\partial u}{\partial x} + v\frac{\partial u}{\partial y} + w\frac{\partial u}{\partial z} = \nu_{hnf}\left(\frac{1}{\xi} + 1\right)\frac{\partial^2 u}{\partial z^2} - \frac{\sigma_{hnf}}{\rho_{hnf}}\frac{B^2}{1+m^2}(u - mv) \quad (5)$$

$$u\frac{\partial v}{\partial x} + v\frac{\partial v}{\partial y} + w\frac{\partial v}{\partial z} = \nu_{hnf}\left(\frac{1}{\xi} + 1\right)\frac{\partial^2 v}{\partial z^2} - \frac{\sigma_{hnf}}{\rho_{hnf}}\frac{B^2}{1+m^2}(v + mu) \quad (6)$$

$$u\frac{\partial T}{\partial x} + v\frac{\partial T}{\partial y} + w\frac{\partial T}{\partial z} + \kappa_e\lambda_e = \alpha_m\frac{\partial^2 T}{\partial z^2} + \tau\left(T_z\frac{\partial C}{\partial z} + \frac{D_T}{T_\infty}\left(\frac{\partial T}{\partial z}\right)^2\right) \quad (7)$$

$$u\frac{\partial C}{\partial x} + v\frac{\partial C}{\partial y} + w\frac{\partial C}{\partial z} + \kappa_c\lambda_c = D_B\frac{\partial^2 C}{\partial z^2} + \frac{D_T}{T_\infty}\frac{\partial^2 C}{\partial z^2} \quad (8)$$

https://doi.org/10.1021/acsomega.2c07750
ACS Omega 2023, 8, 10991−11002

where κ_e and κ_c are the Cattaneo−Christov steady relations, given by[61]

$$\kappa_e = u^2 \frac{\partial^2 T}{\partial z^2} + v^2 \frac{\partial^2 T}{\partial y^2} + w^2 \frac{\partial^2 T}{\partial z^2} + 2\left(uv \frac{\partial^2 T}{\partial xy} + vw \frac{\partial^2 T}{\partial yz} + uw \frac{\partial^2 T}{\partial xz}\right) + \left(u \frac{\partial u}{\partial x} + v \frac{\partial u}{\partial y} + w \frac{\partial u}{\partial z}\right)\frac{\partial T}{\partial x} + \left(u \frac{\partial v}{\partial x} + v \frac{\partial v}{\partial y} + w \frac{\partial v}{\partial z}\right)\frac{\partial T}{\partial y} + \left(u \frac{\partial w}{\partial x} + v \frac{\partial w}{\partial y} + w \frac{\partial w}{\partial z}\right)\frac{\partial T}{\partial z} \quad (9)$$

$$\kappa_c = u^2 \frac{\partial^2 C}{\partial x^2} + v^2 \frac{\partial^2 C}{\partial y^2} + w^2 \frac{\partial^2 C}{\partial z^2} + 2\left(uv \frac{\partial^2 C}{\partial xy} + vw \frac{\partial^2 C}{\partial yz} + uw \frac{\partial^2 C}{\partial xz}\right) + \left(u \frac{\partial u}{\partial x} + v \frac{\partial u}{\partial y} + w \frac{\partial u}{\partial z}\right)\frac{\partial C}{\partial x} + \left(u \frac{\partial v}{\partial x} + v \frac{\partial v}{\partial y} + w \frac{\partial v}{\partial z}\right)\frac{\partial C}{\partial y} + \left(u\frac{\partial w}{\partial x} + v \frac{\partial w}{\partial y} + w \frac{\partial w}{\partial z}\right)\frac{\partial C}{\partial z} \quad (10)$$

Here, ρ is the density, u, v, and w are the components, ν is the viscosity, τ is the heat capacity ratio, $\xi = \frac{\mu_b(2\pi)^{0.5}}{p_y}$ is the Casson parameter, and D_T is the thermophoretic parameter. As per the geometry chosen, the boundary restrictions under the imposed assumptions can be given as

$$u = u_w, \quad v = v_w, \quad w = w_0 e^{((x+y)/2l)}, \quad T - T_w = 0, \quad C - C_w = 0, \quad \text{as } z \to 0 \quad (11a)$$

$$u \to 0, \quad v \to 0, \quad C \to C_\infty, \quad T \to T_\infty \quad \text{as } z \to \infty \quad (11b)$$

where $w_0 = -\left(\frac{c\nu_f}{2l}\right)^{0.5} S_1$, in which S_1 represents the suction or injection case demonstrates the flux of mass. The following similarity variables are introduced:[61]

$$u = ce^{((x+y)/2l)}f', \quad v = de^{((x+y)/2l)}g', \quad w = -\left(\frac{c\nu_f}{2l}\right)^{0.5} e^{((x+y)/2l)}(f + g + \eta f' + \eta g'), \quad T - T_\infty = T_0 e^{(a(x+y)/2l)}, \quad C - C_\infty = C_0 e^{(a(x+y)/2l)}, \ \eta = \left(\frac{c}{2l\nu_f}\right)^{0.5} e^{((x+y)/2l)}, \quad T - T_\infty = (T_f - T_\infty)\theta(\eta) \quad (12)$$

Here, the prime represents the derivative with respect to η.

Using eq 12 in eqs 4−11b, we have[72,74]

$$\left(\frac{1}{\xi} + 1\right)f''' + \frac{\frac{\rho_{hnf}}{\rho_f}}{\frac{\mu_{hnf}}{\mu_f}}(f''(g + f) - 2f'^2 - 2f'g') - \left(\frac{\frac{\sigma_{hnf}}{\sigma_f}}{\frac{\mu_{hnf}}{\mu_f}}\right)\frac{M}{1 + m^2}(f' - mg') = 0 \quad (13)$$

$$\left(\frac{1}{\xi} + 1\right)g''' + \frac{\frac{\rho_{hnf}}{\rho_f}}{\frac{\mu_{hnf}}{\mu_f}}(g''(g + f) - 2g'^2 - 2f'g') - \left(\frac{\frac{\sigma_{hnf}}{\sigma_f}}{\frac{\mu_{hnf}}{\mu_f}}\right)\frac{M}{1 + m^2}(g' + mf') = 0 \quad (14)$$

$$\frac{\frac{k_{hnf}}{k_f}}{Pr\frac{(\rho C_p)_{hnf}}{(\rho C_p)_f}}\theta'' + \theta'(g + f) - a\theta(g' + f') + \delta_1[(\zeta(f' + g') + (2a + 1)(f + g))(f' + g')\theta' - a((2 + a)(f' + g')^2 - (f'' + g'')(g + f)) \theta - \theta''(g + f)^2] + Nb\phi'\theta' + Nt\theta'^2 = 0 \quad (15)$$

$$\frac{1}{Sc}\left(\phi'' + \frac{Nt}{Nb}\theta''\right) + \phi'(f + g) - a(f' + g')\phi + \delta_2[(\zeta(f' + g') + (2a + 1)(f + g))(f' + g')\phi' - a((a + 2)(f' + g')^2 - (f'' + g'')(f + g)) \phi - (f + g)^2\phi''] = 0 \quad (16)$$

with boundary conditons

$$f = 0 = g, \quad f' = 1, \quad g' = \gamma, \quad \theta = 1, \quad \varphi = 1 \quad \text{at } \zeta = 0 \quad (17a)$$

$$f' \to 0, \quad g' \to , \quad \theta \to 0, \quad \varphi \to 0 \quad \text{as } \zeta \to \infty \quad (17b)$$

where $M = \frac{2L\sigma_f B_0{}^2}{\rho C_p}$, $Pr = \frac{\nu_f}{\alpha_f}$, m, $Sc = \frac{\nu}{D_B}$

$$Nb = \frac{\tau D_B(C_w - C_\infty)}{\nu}$$

$$Nt = \frac{\tau D_T(T_w - T_\infty)}{\nu T_\infty}$$

$\gamma = \frac{d}{c}$, $\delta_1 = \lambda_e a$, and $\delta_2 = \lambda_c a$ represent the magnetic parameter, Prandtl number, Hall current parameter, Schmidt number, Brownian motion parameter, thermophoretic parameter, stretching ratio, and thermal and concentration variables for energy and mass flows, respectively. In like manner the HN density, specific heat, and viscosity are denoted by ρ_{hnf}, $(\rho C_p)_{hnf}$ and μ_{hnf} respectively. The basic hybrid nanofluid models are defined as[75]

$$\frac{k_{hnf}}{k_{bf}} = (1 - \Phi_2) + 2\Phi_2\left(\frac{k_{m2}}{k_{m2} - k_{bf}}\right)\ln\left(\frac{k_{m2} + k_{bf}}{2k_{bf}}\right) \quad (18a)$$

https://doi.org/10.1021/acsomega.2c07750
ACS Omega 2023, 8, 10991−11002

$$\frac{k_{bf}}{k_f} = (1 - \Phi_1) + 2\Phi_1\left(\frac{k_{m1}}{k_{m1} - k_f}\right)\ln\left(\frac{k_{m1} + k_f}{2k_f}\right) \tag{18b}$$

$$\frac{\sigma_{hnf}}{\sigma_{bf}} = \left[1 + \frac{3\left(\frac{\sigma_{m2}}{\sigma_{bf}} - 1\right)\Phi_2}{\left(\frac{\sigma_{m2}}{\sigma_{bf}} + 2\right) - \left(\frac{\sigma_{m2}}{\sigma_{bf}} - 1\right)\Phi_2}\right] \tag{19a}$$

$$\frac{\sigma_{bf}}{\sigma_f} = \left[1 + \frac{3\left(\frac{\sigma_{m1}}{\sigma_f} - 1\right)\Phi_1}{\left(\frac{\sigma_{m1}}{\sigma_f} + 2\right) - \left(\frac{\sigma_{m1}}{\sigma_f} - 1\right)\Phi_1}\right] \tag{19b}$$

$$\frac{(\rho C_p)_{hnf}}{(\rho C_p)_f} = \left[(1 - \Phi_2)\left(1 - \left(1 - \frac{(\rho C_p)_{m1}}{(\rho C_p)_f}\right)\Phi_1\right) + \Phi_2\frac{(\rho C_p)_{m2}}{(\rho C_p)_f}\right] \tag{20}$$

$$\frac{\mu_{hnf}}{\mu_f} = \frac{1}{(1 - \Phi_1)^{2.5}(1 - \Phi_2)^{2.5}} \tag{21}$$

$$\frac{\rho_{hnf}}{\rho_f} = \left[(1 - \Phi_2)\left(1 - \left(1 - \frac{\rho_{m1}}{\rho_f}\right)\Phi_1\right) + \Phi_2\frac{\rho_{m2}}{\rho_f}\right] \tag{22}$$

The important engineering parameters are

$$C_{fx}(2Re_x)^{1/2} = \frac{\mu_{hnf}}{\mu_f}f''(0) \tag{23}$$

$$C_{fy}(2Re_y)^{1/2} = \frac{\mu_{hnf}}{\mu_f}\left(\frac{d}{c}\right)^{-1.5}g''(0) \tag{24}$$

$$Sh_x(Re_x)^{-1/2} = -\phi'(0) \tag{25}$$

$$Nu_x(Re_x)^{-1/2} = -\frac{k_{hnf}}{k_f}\theta'(0) \tag{26}$$

here $Re_x = \frac{u_w x}{\nu}$ and $Re_y = \frac{V_w y}{\nu}$ are Reynolds numbers. Table 1 tabulates the properties of the components of the chosen HN.

Table 1. Nanomaterials and Base Fluid Properties[61,76]

property	Ag	ZnO	Casson fluid
k (W/(m K))	429	19	0.6376
C_p (J/(kg K))	235	540	4175
ρ (kg/m^3)	10500	5606	989

3. SOLUTION OF THE PROBLEM USING THE HOMOTOPY ANALYSIS METHOD (HAM)

This particular section deals with the solution of the reduced system of eqs 13−17b. We will use the semianalytical method HAM for the solution. The idea behind the use of this procedure is its fast convergence and degree of freedom in choosing the initial guess. This method was originally introduced by Liao[77] by using the concept of homotopy. He established a mapping given in eq 27, in two continuous functions in the topological spaces $\bar{X}$ and $\bar{Y}$.[78]

$$\tilde{\Psi}: \bar{X} \times [0, 1] \rightarrow \bar{Y} \tag{27}$$

Here, $\tilde{\Psi}[\bar{X}, 0] = \xi_1(\bar{X})$ and $\tilde{\Psi}[\bar{X}, 1] = \xi_2(\bar{X})$ holds $\forall\, \bar{x} \in \bar{X}$.

4. RESULTS AND DISCUSSION

The results achieved by solving the above equations through HAM are displayed through graphs and tables here. The graphs in Figures 2−19 show the effects of different quantities on the state functions. The quantities of engineering importance are displayed in Tables 2 and 3.

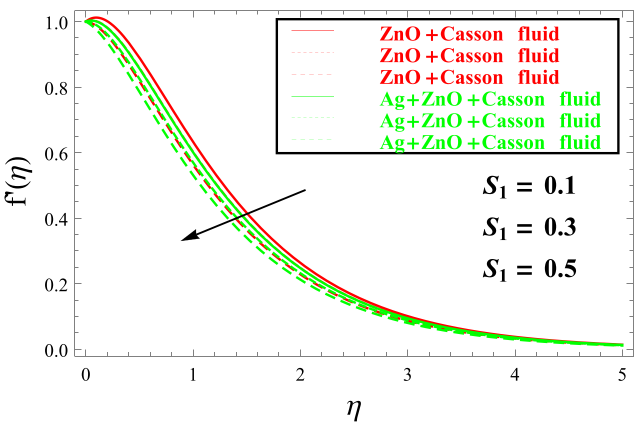

Figure 2. $f'(\eta)$ variation with S_1.

Table 2. Computed Values of C_{fx} and C_{fy} with Varying (γ)

	γ				
	0.2	0.4	0.6	0.8	1.0
$-C_{fx}$	1.03012	1.06423	1.09045	1.22346	1.12778
$-C_{fy}$	2.12532	1.78099	1.50623	1.29478	1.19564

Table 3. Computation of $\theta'(0)$ and $\phi'(0)$ with Changing δ_1 and δ_2

	δ_1, δ_2				
	0.0	0.2	0.4	0.6	0.8
$-\theta'(0)$	0.49043	0.50881	0.51841	0.52961	0.52986
$-\phi'(0)$	0.50984	0.50982	0.50899	0.52012	0.52982

The influence of mass flux S_1 over the velocity gradient $f'(\eta)$ of the selected nanofluid (ZnO + Casson fluid) and HN (Ag + ZnO + Casson fluid) is portrayed in Figure 2. The S_1 parameter values are 0.1, 0.3, and 0.5. It is evident from Figure 2 that the addition of Ag to a simple nanofluid reduces the $f'(\eta)$ profile in comparison with the simple nanofluid. Furthermore, the increasing γ strength drops the velocity profile of both fluids. The drop with enhancing η is more prominent at smaller values of η as displayed by the greater distance between these curves. The separation in the curves decreases at higher η values. Both fluids follow approximately the same pattern. It is therefore concluded that the augmenting flux reduces the $f'(\eta)$ distribution.

The dynamics of both fluids for changing magnetic flux strength M are exhibited in Figure 3. The M values are 0.1, 0.5, and 0.9. Figure 3 displays that the enhancing strength of M causes a drop in $f'(\eta)$ distribution. The reduction in $f'(\eta)$ is higher for middle η values. The separation in the curves depreciates with enhancing η. The increasing M causes a

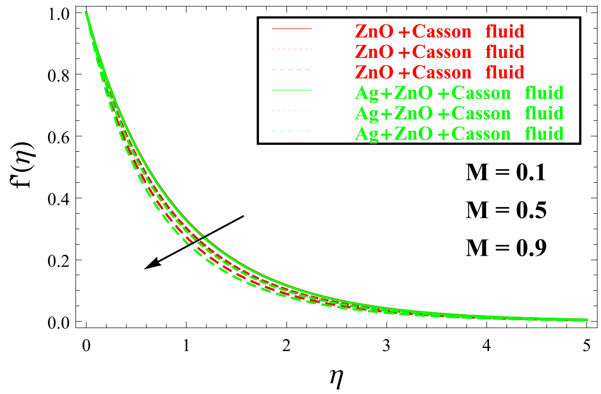

Figure 3. $f'(\eta)$ variation with M.

decrease in $f'(\eta)$ at a higher rate in the HN in comparison with the normal nanofluid. Thus, the augmenting Lorentz force due to high M restricts the velocity distribution.

The $f'(\eta)$ dependence on m is exhibited in Figure 4. The m values are 0.1, 0.5, and 0.9. Figure 4 exhibits that the rising

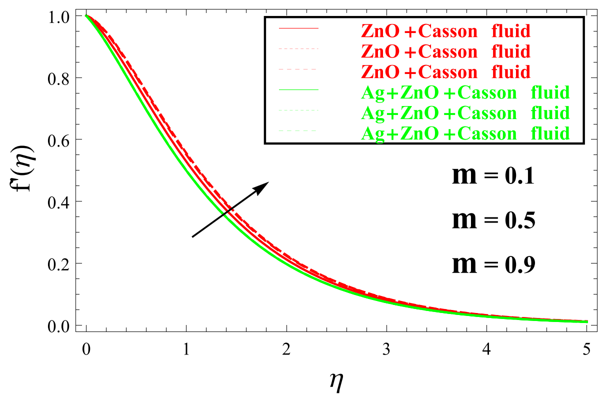

Figure 4. $f'(\eta)$ variation with m.

strength of m augments $f'(\eta)$ for both fluids. The uplift is higher at intermediate η values. Thus, the higher values of m augment the velocities of both fluids.

The $f'(\eta)$ variation with the changing strength of the stretching ratio γ is graphed in Figure 5. The γ values are 0.1, 0.5, and 0.9. Figure 5 shows that larger γ causes $f'(\eta)$

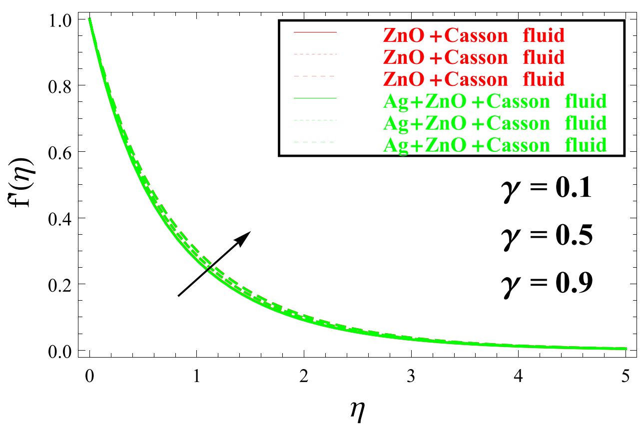

Figure 5. Dependence of $f'(\eta)$ on γ.

enhancement. The overlapping profiles of both fluids show that the rising γ has similar effects on the fluid velocity.

The influence of Casson fluid parameter (ξ) over the velocity gradient is displayed in Figure 6. It is clear that $f'(\eta)$

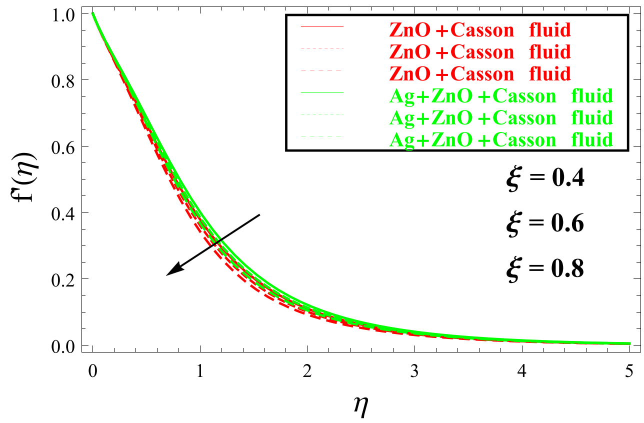

Figure 6. $f'(\eta)$ dependence on ξ.

falls with enhancing ξ. Physically, the larger the Casson fluid parameter, the more viscous is the fluid. Furthermore, the viscosity augments the elasticity of the HN that causes the decline of the momentum boundary layer.

The impacts of S_1 and γ over $g'(\eta)$ are plotted in Figures 7 and 8, respectively. The S_1 values are 0.1, 0.3, and 0.5, and

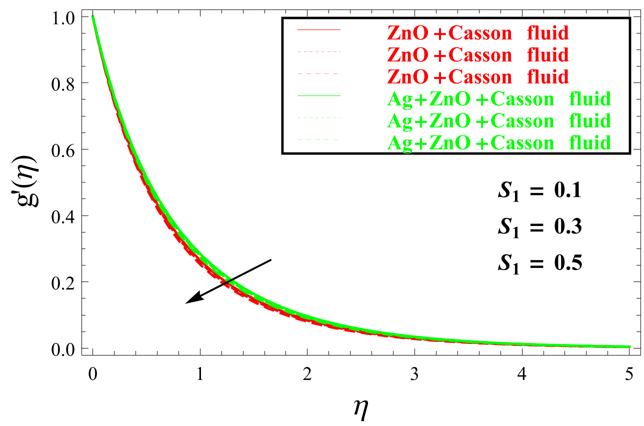

Figure 7. $g'(\eta)$ variation with S_1.

those of γ are 0.1, 0.5, and 0.9. It is evident from Figure 7 that the addition of Ag to the simple nanofluid drops the $g'(\eta)$ profile. Furthermore, increasing γ causes mitigation of the vertical component of the velocity gradient. The drops in the profiles of both fluids have similar dependences on the mass flux parameter. The augmenting γ causes enhancement of the $g'(\eta)$ profile for both fluids as exhibited in Figure 8. The enhancement rate is higher for the HN in comparison with the simple nanofluid. Thus, the addition of Ag drastically changes the $g'(\eta)$ profile. The separation between the two profiles with augmenting γ is more obvious at the central region of the graph.

The impact of ξ is exhibited in Figure 9 over $g'(\eta)$. The enhancement in ξ increases the thickness of the fluid parameter, which further flattens along the y-axis. The viscosity

https://doi.org/10.1021/acsomega.2c07750
ACS Omega 2023, 8, 10991−11002

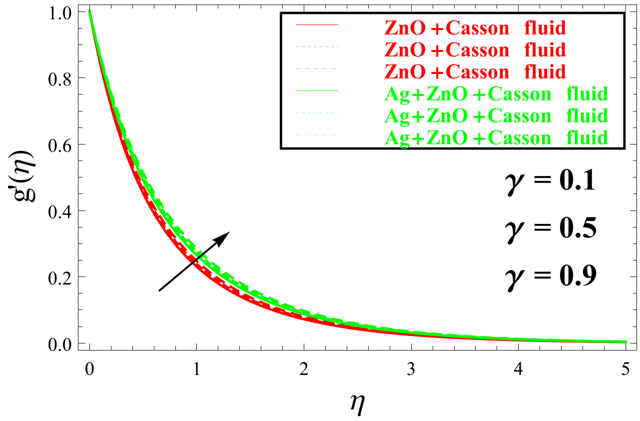

Figure 8. Variation in $g'(\eta)$ with γ.

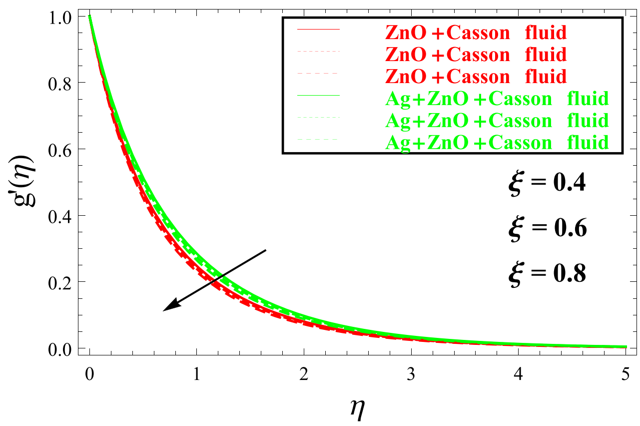

Figure 9. Dependence of $f'(\eta)$ on ξ.

of the fluid enhances, which further slows down the motion; as a result the momentum boundary layer falls.

The variations of temperature $\theta(\eta)$ of both fluids with changing Pr and Nt are graphed in Figures 10 and 11, respectively. The chosen values of Pr are 0.7, 1.1, and 1.5. Figure 10 displays that the addition of Ag with the simple nanofluid raises the temperature distribution of the resultant HN. In addition, the temperature of both fluids mitigates with rising Pr values. The drop in temperature displays a strange dependence on rising Pr. At smaller Pr, the temperature of the simple nanofluid drops quickly in comparison with HN. The temperature drop enhances with increasing Pr. Hence the lower thermal diffusivity due to higher Pr reduces the temperature of both fluids. Figure 11 depicts the effect of augmenting thermophoresis has on the fluid temperature. The increase in temperature with rising Nt is greater for the HN. The temperature enhancement is more drastic at intermediate η values.

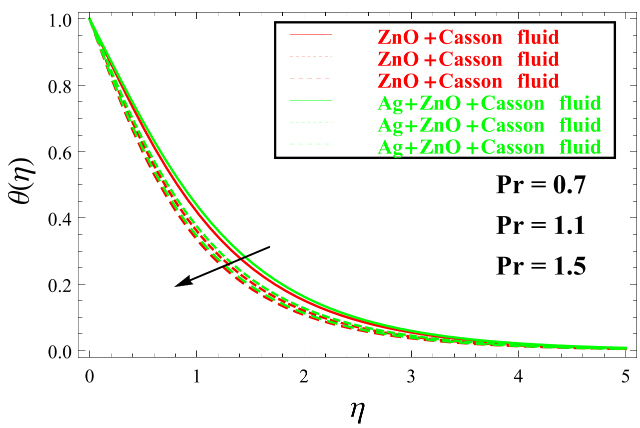

Figure 10. $\theta(\eta)$ dependence on Pr.

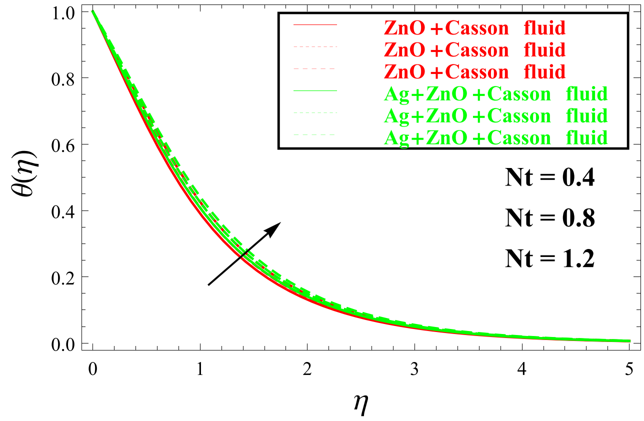

Figure 11. Variation in $\theta(\eta)$ with Nt.

The variations of $\theta(\eta)$ with augmenting Nb, γ, and δ_1 are plotted in Figures 12, 13, and 14, respectively. Figure 12 shows

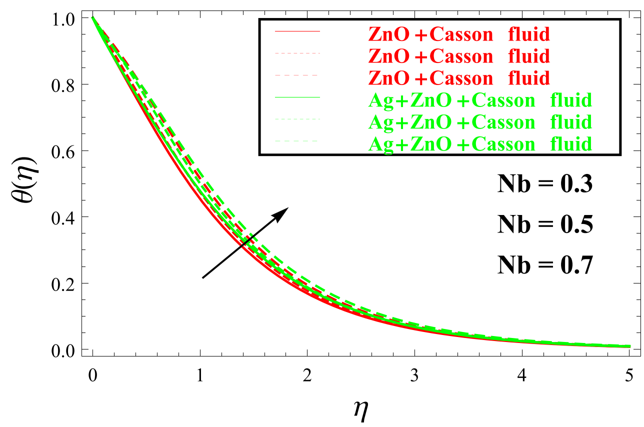

Figure 12. Impact of variation in Nb on $\theta(\eta)$.

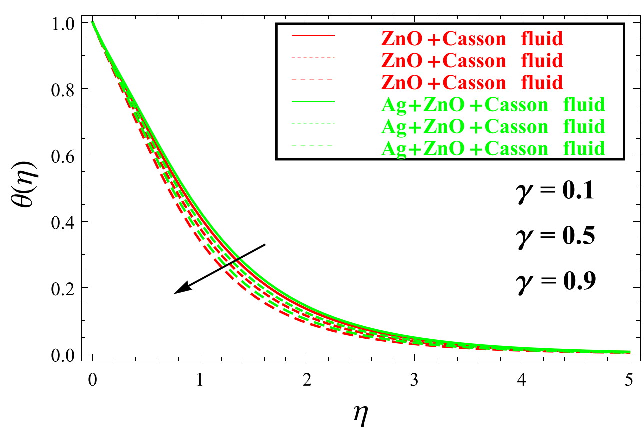

Figure 13. Variation in $\theta(\eta)$ with γ.

https://doi.org/10.1021/acsomega.2c07750
ACS Omega 2023, 8, 10991−11002

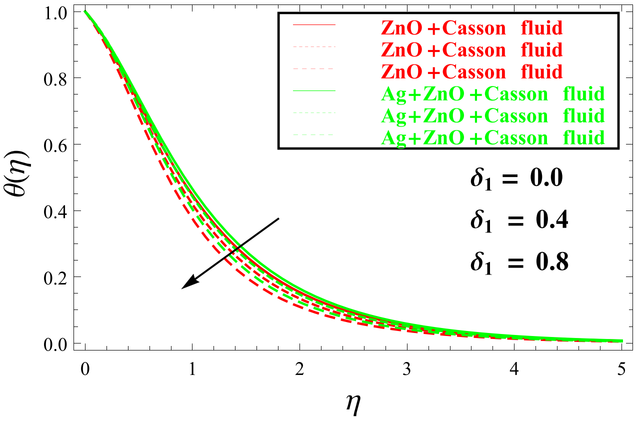

Figure 14. $\theta(\eta)$ dependence on δ_1.

that the enlarging randomness due to larger *Nb* augments the temperature. The enhancement in temperature of HN is higher with augmenting *Nb* in comparison with the nanofluid. The increasing γ reduces the temperature as displayed in Figure 13. The drop displays almost the same pattern for both fluids. The difference is more obvious at intermediate η values. The increasing δ_1 also displays a reduction in $\theta(\eta)$. The drop rates for both fluids follow almost the same trend. Thus, the increasing relaxation in thermal energy causes reduction of the temperature of both fluids.

The fluid concentration ($\phi(\eta)$) variations with the increasing mass flux relaxation parameter (δ_2) and γ values are exhibited in Figures 15 and 16, respectively. The δ_2 values

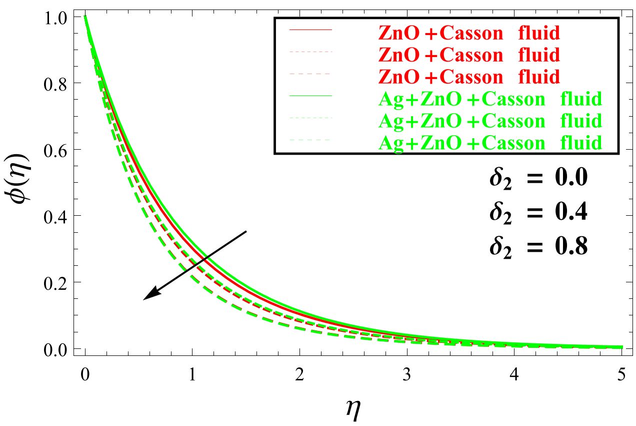

Figure 15. Influence of variation in δ_2 on $\phi(\eta)$.

are 0.0, 0.4, and 0.8, whereas the γ values are 0.1, 0.5, and 0.9. The augmenting δ_2 drops the temperature of the fluids. Initially, the drop is higher for the nanofluid. As δ_2 increases, the drop rate enhances as is evident from the increasing distance between the curves. At the largest δ_2, the drop in concentration for the hybrid nanofluid becomes larger as compared to the simple nanofluid. The increasing γ also causes a fall in $\phi(\eta)$ as displayed in Figure 16. The decline in the HN concentration is higher than that in the simple nanofluid.

The variations of ϕ with enhancing *Nb*, *Nt*, and *Sc* are exhibited in Figures 17, 18, and 19, respectively. The chosen values of *Nb* are 0.3, 0.5, and 0.7. Figure 17 shows a complex dependence of $\phi(\eta)$ with changing *Nb*. At smaller η, the concentration first enhances, reaches a maximum, and then

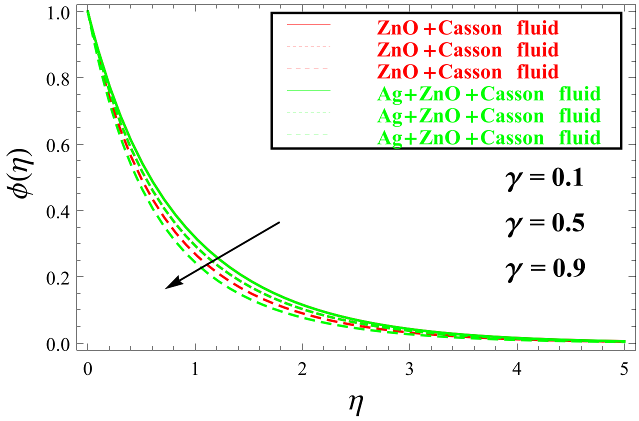

Figure 16. Impact of γ on $\phi(\eta)$.

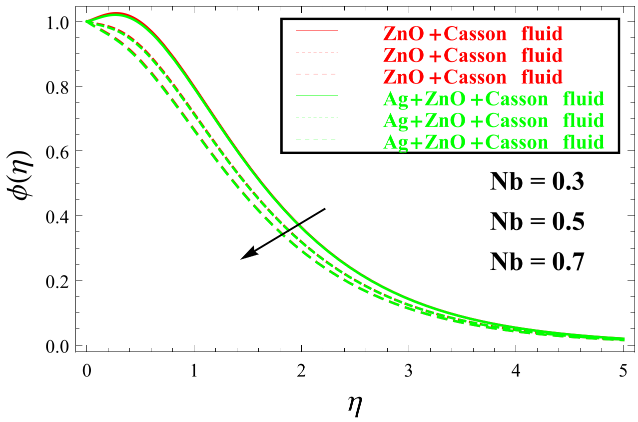

Figure 17. *Nb* impact on $\phi(\eta)$.

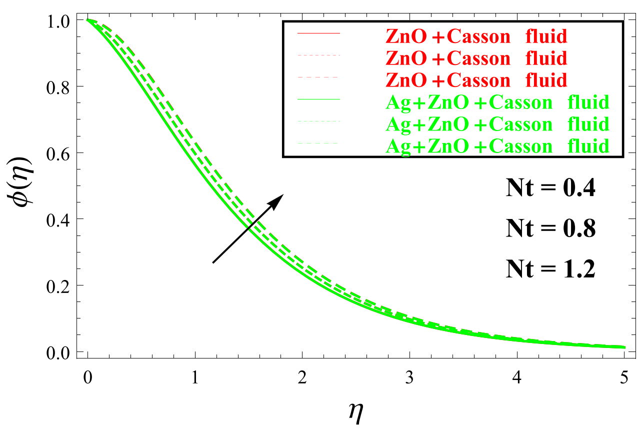

Figure 18. Impact of variation in *Nt* on $\phi(\eta)$.

decreases with higher η values. The concentration drop depreciates with the larger randomness due to larger *Nb* values as shown by the mitigating spacing of the curves. The enhancing thermophoresis due to higher values of *Nt* results an increase in $\phi(\eta)$. The increasing rate is more obvious at smaller η. The increasing *Nt* affects the fluid concentrations of the fluids exactly in the same manner as cleared from the overlapping curves. The effect of varying *Sc* over $\phi(\eta)$ is depicted in Figure 19. The *Sc* values are 0.4, 1.0, and 1.6. Figure 19 displays a reduction in $\phi(\eta)$. The drop for the nanofluid is higher with the enhancing *Sc* than the drop for

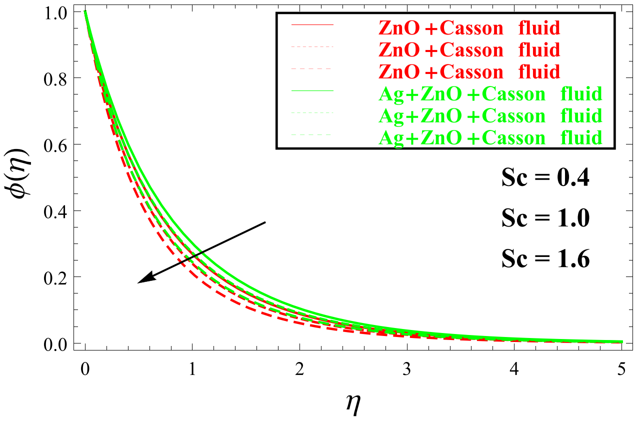

Figure 19. Variation in $\phi(\eta)$ with *Sc*.

HN. Therefore, the enhancing viscosity due to higher values of *Sc* changes the $\phi(\eta)$ profile of nanofluid more drastically.

Figure 20 displays the variation of $\phi(\eta)$ with changing ξ. It displays a decreasing trend with the higher ξ strength.

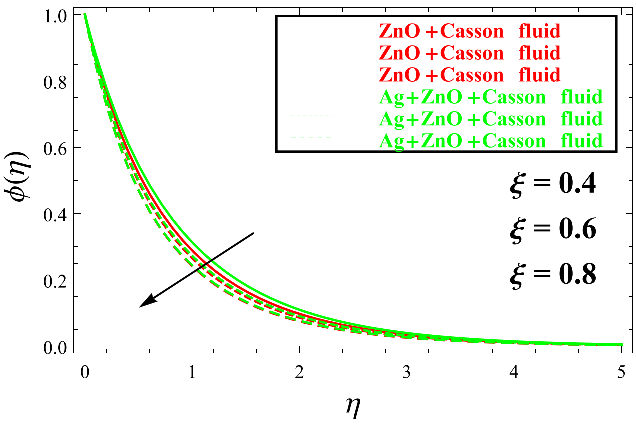

Figure 20. Impact of ξ on $\phi(\eta)$.

Physically, the larger values decline the thickness of the momentum of the boundary layer as the viscosity increases as a result the intermolecular bond increase that results in the decline of the concentration profile.

5. TABLES DISCUSSION

This portion expresses the numerical computation of coefficients of interest in Tables 2 and 3 with changing values of the selected parameters namely, γ, δ_1, and δ_2.[61] Table 2 exhibits the opposite behavior with rising γ for the coefficient of friction. Table 3 displays that the heat transfer enhances with the increasing relaxation parameter and displays a similar behavior for mass transfer.

6. CONCLUSIONS

This section is devoted to the results obtained for the hybrid Casson nanofluid flow. Here, we explained the combination of Casson fluid with ZnO and with Ag + ZnO for the formation of nanofluid and hybrid nanofluid. The CCDD model is taken into account for modeling the problem. The problem is solved with the semianalytical method HAM, and the results are plotted for the impacts of various parameters. The results show that the common nanofluid is weaker than the hybrid nanofluid. The main outcomes of this work are summarized as follows:

- The velocity gradients fall with increasing values of the dimensionless mass flux (S_1).
- The Casson fluid parameter ξ with its increasing trend decreases the velocity f' and concentration ϕ profiles. An opposite trend has been reported for g'.
- The larger values of the Prandtl number (Pr) result in a decline of the thermal boundary layer.
- Nt and Nb increase the concentration of the moving nanoparticles, and as a result with its increasing value, heat transport becomes dominant.
- The Hall current produced due to the influence of the magnetic parameter and the mass flux with its larger values decrease the velocity profile.
- Both the thermal and concentration profiles decline with larger values of the thermal and concentration relaxation parameters.
- The ratio parameter γ shows an opposite trend for both the temperature and concentration profiles.

ASSOCIATED CONTENT

Data Availability Statement

The data used to support the findings of this study are available within the article.

AUTHOR INFORMATION

Corresponding Author

Asad Ullah − *Department of Mathematical Sciences, University of Lakki Marwat, Lakki Marwat 28420, Pakistan;* orcid.org/0000-0002-4361-7786; Email: asad@ulm.edu.pk

Authors

Ramadan A. ZeinEldin − *Deanship of Scientific Research, King AbdulAziz University, Jeddah 21589, Saudi Arabia*

Hamiden Abd El-Wahed Khalifa − *Department of Operations and Management Research, Faculty of Graduate Studies for Statistical Research, Cairo University, Giza 12613, Egypt; Department of Mathematics, College of Science and Arts, Qassim University, Al-Badaya 51951, Saudi Arabia*

Complete contact information is available at: https://pubs.acs.org/10.1021/acsomega.2c07750

Author Contributions

Conceptualization: R.A.Z, H.A.E.-W.K., and A.U. Software: R.A.Z., H.A.E.-W.K., and A.U. Writing—original draft preparation: A.U., R.A.Z., and H.A.E.-W.K. Writing—review and editing: H.A.E.-W.K., R.A.Z., and A.U. Formal analysis: H.A.E.-W.K. and R.A.Z. Validation: H.A.E.-W.K., A.U., and R.A.Z. Methodology: R.A.Z., A.U., and H.A.E.-W.K. Investigation: H.A.E.-W.K. and A.U. Resources: A.U. and R.A.Z. Project administration: R.A.Z., A.U., and H.A.E.-W.K. Funding Acquisition: R.A.Z. and H.A.E.-W.K. All authors have read and agreed to the final version of the manuscript.

Funding

This research work was funded by Institutional Fund projects under Grant No. (IFPIP: 1588-305-1443). The authors gratefully acknowledge the technical and financial support provided by the Ministry of Education and King Abdulaziz University, DSR, Jeddah, Saudi Arabia.

Notes

The authors declare no competing financial interest.

■ ACKNOWLEDGMENTS

This research work was funded by Institutional Fund projects (IFPIP: 1588-305-1443). The authors gratefully acknowledge technical and financial support provided by the Ministry of Education and King Abdulaziz University, DSR, Jeddah, Saudi Arabia.

■ REFERENCES

(1) Choi, S. U. S.; Eastman, J. A. *Enhancing Thermal Conductivity of Fluids with Nanoparticles*; technical report; Argonne National Laboratory (ANL): Argonne, IL, 1995.
(2) Said, Z.; Sundar, L. S.; Tiwari, A. K.; Ali, H. M.; Sheikholeslami, M.; Bellos, E.; Babar, H. Recent advances on the fundamental physical phenomena behind stability, dynamic motion, thermophysical properties, heat transport, applications, and challenges of nanofluids. *Phys. Rep.* **2022**, *946*, 1−94.
(3) Rashidi, M. M.; Ghahremanian, S.; Toghraie, D.; Roy, P. Effect of solid surface structure on the condensation flow of argon in rough nanochannels with different roughness geometries using molecular dynamics simulation. *International Communications in Heat and Mass Transfer* **2020**, *117*, 104741.
(4) Mansoury, D.; Ilami Doshmanziari, F.; Rezaie, S.; Rashidi, M. M. Effect of al2o3/water nanofluid on performance of parallel flow heat exchangers. *J. Therm. Anal. Calorim.* **2019**, *135* (1), 625−643.
(5) Hatami, M.; Zhou, J.; Geng, J.; Song, D.; Jing, D. Optimization of a lid-driven t-shaped porous cavity to improve the nanofluids mixed convection heat transfer. *J. Mol. Liq.* **2017**, *231*, 620−631.
(6) Turkyilmazoglu, M. Single phase nanofluids in fluid mechanics and their hydrodynamic linear stability analysis. *Computer Methods and Programs in Biomedicine* **2020**, *187*, 105171.
(7) Liang, G.; Mudawar, I. Review of single-phase and two-phase nanofluid heat transfer in macro-channels and micro-channels. *Int. J. Heat Mass Transfer* **2019**, *136*, 324−354.
(8) Kumar, P.; Poonia, H.; Ali, L.; Areekara, S. The numerical simulation of nanoparticle size and thermal radiation with the magnetic field effect based on tangent hyperbolic nanofluid flow. *Case Studies in Thermal Engineering* **2022**, *37*, 102247.
(9) Jin, C.; Wu, Q.; Yang, G.; Zhang, H.; Zhong, Y. Investigation on hybrid nanofluids based on carbon nanotubes filled with metal nanoparticles: Stability, thermal conductivity, and viscosity. *Powder Technol.* **2021**, *389*, 1−10.
(10) Daniel, Y. S.; Aziz, Z. A.; Ismail, Z.; Salah, F. Thermal radiation on unsteady electrical mhd flow of nanofluid over stretching sheet with chemical reaction. *Journal of King Saud University-Science* **2019**, *31* (4), 804−812.
(11) Yıldız, Ç.; Arıcı, M.; Karabay, H. Comparison of a theoretical and experimental thermal conductivity model on the heat transfer performance of al2o3-sio2/water hybrid-nanofluid. *Int. J. Heat Mass Transfer* **2019**, *140*, 598−605.
(12) Asokan, N.; Gunnasegaran, P.; Wanatasanappan, V. V. Experimental investigation on the thermal performance of compact heat exchanger and the rheological properties of low concentration mono and hybrid nanofluids containing al2o3 and cuo nanoparticles. *Thermal Science and Engineering Progress* **2020**, *20*, 100727.
(13) Ho, C. J.; Liu, Y.-C.; Yang, T.-F.; Ghalambaz, M.; Yan, W.-M. Convective heat transfer of nano-encapsulated phase change material suspension in a divergent minichannel heatsink. *Int. J. Heat Mass Transfer* **2021**, *165*, 120717.
(14) Wanatasanappan, V. V.; Abdullah, M. Z.; Gunnasegaran, P. Thermophysical properties of al2o3-cuo hybrid nanofluid at different nanoparticle mixture ratio: An experimental approach. *J. Mol. Liq.* **2020**, *313*, 113458.
(15) Singh Sambyal, M.; Singh, S. K.; Sharma, D. Numerical investigation of heat transfer performance of microchannel with wall-mounted obstacles using hybrid nanofluids. *International Journal of Ambient Energy* **2022**, *43* (1), 7910−7921.
(16) Soltani, F.; Toghraie, D.; Karimipour, A. Experimental measurements of thermal conductivity of engine oil-based hybrid and mono nanofluids with tungsten oxide (wo3) and mwcnts inclusions. *Powder Technology* **2020**, *371*, 37−44.
(17) Boroomandpour, A.; Toghraie, D.; Hashemian, M. A comprehensive experimental investigation of thermal conductivity of a ternary hybrid nanofluid containing mwcnts-titania-zinc oxide/water-ethylene glycol (80:20) as well as binary and mono nanofluids. *Synth. Met.* **2020**, *268*, 116501.
(18) Yan, S.-R.; Toghraie, D.; Abdulkareem, L. A.; Alizadeh, A.; Barnoon, P.; Afrand, M. The rheological behavior of mwcnts−zno/water−ethylene glycol hybrid non-newtonian nanofluid by using of an experimental investigation. *Journal of Materials Research and Technology* **2020**, *9* (4), 8401−8406.
(19) Rostami, S.; Toghraie, D.; Esfahani, M. A.; Hekmatifar, M.; Sina, N. Predict the thermal conductivity of sio2/water−ethylene glycol (50:50) hybrid nanofluid using artificial neural network. *J. Therm. Anal. Calorim.* **2021**, *143* (2), 1119−1128.
(20) Khan, I. Shape effects of mos2 nanoparticles on mhd slip flow of molybdenum disulphide nanofluid in a porous medium. *J. Mol. Liq.* **2017**, *233*, 442−451.
(21) Chamkha, A. J.; Ismael, M. A. Magnetic field effect on mixed convection in lid-driven trapezoidal cavities filled with a cu−water nanofluid with an aiding or opposing side wall. *Journal of Thermal Science and Engineering Applications* **2016**, *8* (3), 031009.
(22) Alsabery, A. I.; Ismael, M. A.; Chamkha, A. J.; Hashim, I. Mixed convection of al2o3-water nanofluid in a double lid-driven square cavity with a solid inner insert using buongiorno's two-phase model. *Int. J. Heat Mass Transfer* **2018**, *119*, 939−961.
(23) Muhammad, T.; Alamri, S. Z.; Waqas, H.; Habib, D.; Ellahi, R. Bioconvection flow of magnetized carreau nanofluid under the influence of slip over a wedge with motile microorganisms. *J. Therm. Anal. Calorim.* **2021**, *143*, 945−957.
(24) Siddiqui, A. A.; Sheikholeslami, M. Tio 2-water nanofluid in a porous channel under the effects of an inclined magnetic field and variable thermal conductivity. *Applied Mathematics and Mechanics* **2018**, *39*, 1201−1216.
(25) Sheikholeslami, M. Influence of magnetic field on al2o3-h2o nanofluid forced convection heat transfer in a porous lid driven cavity with hot sphere obstacle by means of lbm. *J. Mol. Liq.* **2018**, *263*, 472−488.
(26) Seyyedi, S. M.; Hashemi-Tilehnoee, M.; Asghar, Z.; Waqas, M.; Ganji, D. D.; Dogonchi, A. S. D. A computational framework for natural convective hydromagnetic flow via inclined cavity: an analysis subjected to entropy generation. *J. Mol. Liq.* **2019**, *287*, 110863.
(27) Khan, A.; Shah, Z.; Alzahrani, E.; Islam, S. Entropy generation and thermal analysis for rotary motion of hydromagnetic casson nanofluid past a rotating cylinder with joule heating effect. *International Communications in Heat and Mass Transfer* **2020**, *119*, 104979.
(28) Sakiadis, B. C. Boundary-layer behavior on continuous solid surfaces: I. boundary-layer equations for two-dimensional and axisymmetric flow. *AIChE J.* **1961**, *7* (1), 26−28.
(29) Crane, L. J. Flow past a stretching plate. *J. Appl. Math. Phys. (ZAMP)* **1970**, *21* (4), 645−647.
(30) Gupta, P. S.; Gupta, A. S. Heat and mass transfer on a stretching sheet with suction or blowing. *Canadian journal of chemical engineering* **1977**, *55* (6), 744−746.
(31) Devi, R. L. V. R.; Neeraja, A.; Bhaskar Reddy, N. Radiation effect on mhd slip flow past a stretching sheet with variable viscosity and heat source/sink. *International Journal of Scientific and Innovative Mathematical Research* **2015**, *3*, 8−17.
(32) Magyari, E.; Keller, B. Heat and mass transfer in the boundary layers on an exponentially stretching continuous surface. *J. Phys. D: Appl. Phys.* **1999**, *32* (5), 577.
(33) Wang, C. Y. Liquid film on an unsteady stretching surface. *Quarterly of applied Mathematics* **1990**, *48* (4), 601−610.

(34) Miklavčič, M.; Wang, C. Viscous flow due to a shrinking sheet. *Quarterly of Applied Mathematics* **2006**, *64* (2), 283−290.
(35) Bhattacharyya, K. Boundary layer flow and heat transfer over an exponentially shrinking sheet. *Chin. Phys. Lett.* **2011**, *28* (7), 074701.
(36) Bachok, N.; Ishak, A.; Pop, I. Boundary layer stagnation-point flow and heat transfer over an exponentially stretching/shrinking sheet in a nanofluid. *Int. J. Heat Mass Transfer* **2012**, *55* (25−26), 8122−8128.
(37) Jusoh, R.; Nazar, R.; Pop, I. Magnetohydrodynamic boundary layer flow and heat transfer of nanofluids past a bidirectional exponential permeable stretching/shrinking sheet with viscous dissipation effect. *Journal of Heat Transfer* **2019**, *141* (1), 012406.
(38) Qadeer, M.; Khan, U.; Ahmad, S. Irreversibility analysis for three-dimensional squeezing flow of hybrid nanofluids: a numerical study. *Waves in Random and Complex Media* **2022**, 1−27.
(39) Khan, M. F.; Pervez, A.; Modibbo, U. M.; Chauhan, J.; Ali, I. Flexible fuzzy goal programming approach in optimal mix of power generation for socio-economic sustainability: a case study. *Sustainability* **2021**, *13* (15), 8256.
(40) Tian, S.; Arshad, N. I.; Toghraie, D.; Eftekhari, S. A.; Hekmatifar, M. Using perceptron feed-forward artificial neural network (ann) for predicting the thermal conductivity of graphene oxide-al2o3/water-ethylene glycol hybrid nanofluid. *Case Studies in Thermal Engineering* **2021**, *26*, 101055.
(41) Lu, G.; Wang, Xi.-D.; Duan, Y.-Y. A critical review of dynamic wetting by complex fluids: from newtonian fluids to non-newtonian fluids and nanofluids. *Advances in Colloid and Interface Science* **2016**, *236*, 43−62.
(42) Rauf, A.; Abbas, Z.; Shehzad, S. A. Utilization of maxwell-cattaneo law for mhd swirling flow through oscillatory disk subject to porous medium. *Applied Mathematics and Mechanics* **2019**, *40* (6), 837−850.
(43) Christov, C. I. On frame indifferent formulation of the maxwell−cattaneo model of finite-speed heat conduction. *Mechanics Research Communications* **2009**, *36* (4), 481−486.
(44) Irfan, M.; Khan, M.; Khan, W. A. On model for three-dimensional carreau fluid flow with cattaneo−christov double diffusion and variable conductivity: a numerical approach. *Journal of the Brazilian Society of Mechanical Sciences and Engineering* **2018**, *40* (12), 577.
(45) Iqbal, Z.; Khan, M.; Ahmed, A.; Ahmed, J.; Hafeez, A. Thermal energy transport in burgers nanofluid flow featuring the cattaneo−christov double diffusion theory. *Applied Nanoscience* **2020**, *10* (12), 5331−5342.
(46) Casson, N. A flow equation for pigment-oil suspensions of the printing ink type. In *Rheology of Disperse Systems*; Mill, C. C., Ed.; Pergamon: 1959; pp 84−104.
(47) Bird, R. B.; Dai, G. C.; Yarusso, B. J. The rheology and flow of viscoplastic materials. *Reviews in chemical engineering* **1983**, *1* (1), 1−70.
(48) Mitsoulis, E. Flows of viscoplastic materials: models and computations. *Rheology Reviews*; Binding, D. M., Hudson, N. E., Keunings, R., Eds.; British Society of Rheology: 2007; pp 135−178.
(49) Yasir, M.; Ahmed, A.; Khan, M.; Alzahrani, A. K.; Malik, Z. U.; Alshehri, A. M. Mathematical modelling of unsteady oldroyd-b fluid flow due to stretchable cylindrical surface with energy transport. *Ain Shams Engineering Journal* **2023**, *14* (1), 101825.
(50) Reddy, N. N.; Reddy, Y. D.; Srinivasa Rao, V.; Goud, B. S.; Nisar, K. S. Multiple slip effects on steady mhd flow past a non-isothermal stretching surface in presence of soret, dufour with suction/injection. *International Communications in Heat and Mass Transfer* **2022**, *134*, 106024.
(51) Goud Bejawada, S.; Reddy, Y. D.; Jamshed, W.; Nisar, K. S.; Alharbi, A. N.; Chouikh, R. Radiation effect on mhd casson fluid flow over an inclined non-linear surface with chemical reaction in a forchheimer porous medium. *Alexandria Engineering Journal* **2022**, *61* (10), 8207−8220.
(52) Ramzan, M.; Saeed, A.; Kumam, P.; Ahmad, Z.; Junaid, M. S.; Khan, D. Influences of soret and dufour numbers on mixed convective and chemically reactive casson fluids flow towards an inclined flat plate. *Heat Transfer* **2022**, *51* (5), 4393−4433.
(53) Abdelmalek, Z.; Mahanthesh, B.; Md Basir, Md. F.; Imtiaz, M.; Mackolil, J.; Khan, N. S.; Nabwey, H. A.; Tlili, I. Mixed radiated magneto casson fluid flow with arrhenius activation energy and newtonian heating effects: flow and sensitivity analysis. *Alexandria Engineering Journal* **2020**, *59* (5), 3991−4011.
(54) Khan, U.; Mebarek-Oudina, F.; Zaib, A.; Ishak, A.; Abu Bakar, S.; Sherif, E.-S. M.; Baleanu, D. An exact solution of a casson fluid flow induced by dust particles with hybrid nanofluid over a stretching sheet subject to lorentz forces. *Waves in Random and Complex Media* **2022**, 1−14.
(55) Ahmad, I.; Faisal, M.; Javed, T. Bi-directional stretched nanofluid flow with cattaneo-christov double diffusion. *Results in Physics* **2019**, *15*, 102581.
(56) Rauf, A.; Shehzad, S. A.; Abbas, Z.; Hayat, T. Unsteady three-dimensional mhd flow of the micropolar fluid over an oscillatory disk with cattaneo-christov double diffusion. *Applied Mathematics and Mechanics* **2019**, *40* (10), 1471−1486.
(57) Hayat, T.; Qayyum, S.; Shehzad, S. A.; Alsaedi, A. Chemical reaction and heat generation/absorption aspects in flow of walters-b nanofluid with cattaneo-christov double-diffusion. *Results in Physics* **2017**, *7*, 4145−4152.
(58) Hayat, T.; Aziz, A.; Muhammad, T.; Alsaedi, A. Three-dimensional flow of prandtl fluid with cattaneo-christov double diffusion. *Results in Physics* **2018**, *9*, 290−296.
(59) Nasir, M.; Waqas, M.; Kausar, MS.; Bég, O. A.; Zamri, N. Cattaneo-christov dual diffusive non-newtonian nanoliquid flow featuring nonlinear convection. *Chinese Journal of Physics* **2022**, DOI: 10.1016/j.cjph.2022.05.005.
(60) Ibrahim, W. Three dimensional rotating flow of powell-eyring nanofluid with non-fourier's heat flux and non-fick's mass flux theory. *Results in Physics* **2018**, *8*, 569−577.
(61) ZeinEldin, R. A.; Ullah, A.; Khalifa, H. A. E.-W.; Ayaz, M. Analytical study of the energy loss reduction during three-dimensional engine oil-based hybrid nanofluid flow by using cattaneo−christov model. *Symmetry* **2023**, *15* (1), 166.
(62) Khan, U.; Ahmad, S.; Hayyat, A.; Khan, I.; Nisar, K. S.; Baleanu, D. On the cattaneo−christov heat flux model and oham analysis for three different types of nanofluids. *Applied Sciences* **2020**, *10* (3), 886.
(63) Mabood, F.; Das, K. Outlining the impact of melting on mhd casson fluid flow past a stretching sheet in a porous medium with radiation. *Heliyon* **2019**, *5* (2), No. e01216.
(64) Anwar, T.; Kumam, P.; Watthayu, W. Unsteady mhd natural convection flow of casson fluid incorporating thermal radiative flux and heat injection/suction mechanism under variable wall conditions. *Sci. Rep.* **2021**, *11* (1), 4275.
(65) Sandeep, N.; Sulochana, C.; Ashwinkumar, G. P. Understanding the dynamics of chemically reactive casson liquid flow above a convectively heated curved expanse. *Proceedings of the Institution of Mechanical Engineers, Part C: Journal of Mechanical Engineering Science* **2022**, *236* (24), 11420−11430.
(66) Saleem, S.; Akhtar, S.; Nadeem, S.; Saleem, A.; Ghalambaz, M.; Issakhov, A. Mathematical study of electroosmotically driven peristaltic flow of casson fluid inside a tube having systematically contracting and relaxing sinusoidal heated walls. *Chinese Journal of Physics* **2021**, *71*, 300−311.
(67) Hafez, N. M.; Abd-Alla, A. M.; Metwaly, T. M. N. Influences of rotation and mass and heat transfer on mhd peristaltic transport of casson fluid through inclined plane. *Alexandria Engineering Journal* **2023**, *68*, 665−692.
(68) Alzahrani, A. K.; Abbas, Z.; Ullah, M. Z. Chemically reactive two-phase flow of viscous-casson fluids in a rotating channel. *Alexandria Engineering Journal* **2023**, *62*, 403−413.
(69) Rehman, K. U.; Shatanawi, W.; Laraib, K. Mutual impact of thermal radiations and temperature dependent thermal conductivity on non-newtonian multiple flow regimes. *Case Studies in Thermal Engineering* **2023**, *42*, 102752.

(70) Krishna, M. V.; Swarnalathamma, B. V.; Chamkha, A. J. Investigations of soret, joule and hall effects on mhd rotating mixed convective flow past an infinite vertical porous plate. *Journal of Ocean Engineering and Science* **2019**, *4* (3), 263−275.
(71) Verma, V. K.; Mondal, S. A brief review of numerical methods for heat and mass transfer of casson fluids. *Partial Differential Equations in Applied Mathematics* **2021**, *3*, 100034.
(72) Hayat, T.; Muhammad, T.; Alsaedi, A.; Ahmad, B. Three-dimensional flow of nanofluid with cattaneo−christov double diffusion. *Results in Physics* **2016**, *6*, 897−903.
(73) Shankar, U.; Naduvinamani, N. B. Magnetized impacts of cattaneo-christov double-diffusion models on the time-dependent squeezing flow of casson fluid: A generalized perspective of fourier and fick's laws. *European Physical Journal Plus* **2019**, *134* (7), 344.
(74) Zangooee, M. R.; Hosseinzadeh, K.; Ganj, D. D. Investigation of three-dimensional hybrid nanofluid flow affected by nonuniform mhd over exponential stretching/shrinking plate. *Nonlinear Engineering* **2022**, *11* (1), 143−155.
(75) Turkyilmazoglu, M. On the transparent effects of buongiorno nanofluid model on heat and mass transfer. *European Physical Journal Plus* **2021**, *136* (4), 376.
(76) Algehyne, E. A.; Alharbi, A. F.; Saeed, A.; Dawar, A.; Ramzan, M.; Kumam, P. Analysis of the mhd partially ionized go-ag/water and go-ag/kerosene oil hybrid nanofluids flow over a stretching surface with cattaneo−christov double diffusion model: A comparative study. *International Communications in Heat and Mass Transfer* **2022**, *136*, 106205.
(77) Liao, S.-J. The proposed homotopy analysis technique for the solution of nonlinear problems. Ph.D. Thesis, Shanghai Jiao Tong University, 1992.
(78) Liao, S. Homotopy analysis method: a new analytical technique for nonlinear problems. *Communications in Nonlinear Science and Numerical Simulation* **1997**, *2* (2), 95−100.

https://doi.org/10.1021/acsomega.2c07750
ACS Omega 2023, 8, 10991−11002